First publ. in: Applied Physics / A, Materials Science and Processing, 82 (2006), pp. 489-493

Y.S. DEDKOV[1,✉,*]
M. FONIN[1,2]
U. RÜDIGER[2]
G. GÜNTHERODT[1]

Spin-resolved photoelectron spectroscopy of the MgO/Fe(110) system

[1] II. Physikalisches Institut, Rheinisch-Westfälische Technische Hochschule Aachen, 52056 Aachen, Germany
[2] Fachbereich Physik, Universität Konstanz, 78457 Konstanz, Germany

Received: 24 March 2005/Accepted: 18 October 2005
Published online: 19 November 2005

ABSTRACT The surface structure and electronic properties of ultrathin MgO layers grown on epitaxial Fe(110) films were investigated at room temperature by means of electron diffraction, Auger electron spectroscopy, scanning tunneling microscopy, and spin-resolved photoelectron spectroscopy. The spin polarization at the Fermi level (E_F) of the Fe(110) film decreases sharply with increasing thickness of the MgO layer. This behavior arises from the formation of a thin FeO layer at the MgO(111)/Fe(110) interface, as revealed by structural and spectroscopic investigations. The strong attenuation of the intrinsic spin polarization is qualitatively attributed to the scattering of spin-polarized electrons at the unoccupied *d*-orbitals of Fe^{2+}.

PACS 68.35.-p; 68.55.-a; 73.20.r; 75.70.Cn; 79.60.-I

1 Introduction

The high tunneling magnetoresistance (TMR) values achievable by means of magnetic tunnel junctions (MTJs) [1–5] consisting of two ferromagnetic electrodes separated by a thin insulating layer have attracted strong interest for potential applications in magnetoelectronics [6–8]. According to Julliére's model [9] the magnetoresistance of such MTJs depends only on the spin polarization of the ferromagnetic electrodes used. In contrast, ab initio electronic structure and transport calculations have shown that the magnetoelectronic properties of such devices strongly depend on the structural as well as electronic properties of the insulating layer and the specific termination at the insulator/ferromagnet (I/FM) interface [10–13].

In the last few years, the epitaxial Fe/MgO/Fe(100) MTJ system has been intensively studied. For ideal MTJs with abrupt interfaces between MgO and Fe, the TMR values are predicted to be as high as $\sim 2000\%$ [13]. Recent experiments on Fe(100)/MgO/FeCo [14] and Fe/MgO/Fe [15] MTJs showed TMR values of 60% at 30 K and 100% at 80 K, respectively, which are close to the theoretically predicted value of 75% for the Fe/MgO/Fe system with a FeO layer at the MgO/Fe interface [16]. Up to now there are only few experimental evidences for high TMR effect in fully epitaxial Fe/MgO/Fe(100) MTJs, with magnetoresistance ratio of about 146% [3] and 180% [5] measured at room temperature. However, these values are far away from the theoretically predicted extraordinarily high values of TMR. This fact can be considered as an indirect proof for an iron oxide formation at the inhomogeneous MgO/Fe interface. The surface x-ray diffraction (SXRD) and vibration spectroscopy experiments [17–19] which were carried out on the MgO/Fe(100) system gave direct evidence for the formation of a FeO submonolayer at the interface.

In the present work the crystallographic and electronic structure of the MgO/Fe(110) system was investigated by means of low energy electron diffraction (LEED), scanning tunneling microscopy (STM), Auger electron spectroscopy (AES), and spin- and angle-resolved photoelectron spectroscopy (SPARPES). MgO layers with (111) orientation were epitaxially grown on an Fe(110) surface as described in [20, 21]. The SPARPES experiments show that the spin polarization of photoelectrons at E_F decreases abruptly with increasing MgO layer thickness indicating that the spin scattering of photoelectrons in the MgO overlayer is not the only source of the strong damping. Our observation is thought to be due to the formation of a thin depolarizing FeO layer at the MgO/Fe interface.

2 Experimental details

All experiments were carried out at room temperature in two separate ultra-high vacuum (UHV) systems. The first system for STM measurements with a base pressure of 8×10^{-11} mbar is equipped with LEED optics and a scanning tunneling microscope (Omicron UHV AFM/STM). STM measurements were carried out using electrochemically etched polycrystalline tungsten tips cleaned in vacuo by Ar^+ sputtering. The second system for spin-resolved photoemission analysis is described in detail in [22]. It consists of a UHV chamber equipped with LEED optics and an Auger-electron spectrometer. The SPARPES spectra (He I, $h\nu = 21.2$ eV) were recorded in normal emission by a 180° hemi-spherical energy analyzer connected to a 100 kV Mott detector for spin analysis. The energy resolution was 100 meV and the angle

✉ Fax: +49 351 463 33 457, E-mail: dedkov@physik.phy.tu-dresden.de
Present address: Institut für Festkörperphysik, Technische Universität Dresden, 01062 Dresden, Germany

resolution was ±1°. The spin-resolved measurements were performed at remanence after having applied a magnetic field pulse of approximately 500 Oe along the in-plane $\langle 1\bar{1}0\rangle$ easy axis of the thin Fe(110) film [23].

Clean 50-Å-thick Fe(110) films were prepared in situ by electron-beam evaporation onto a W(110) substrate, while the thickness was simultaneously monitored by a quartz microbalance. The degree of crystalline order of the thin epitaxial Fe(110) films and the MgO overlayer was checked by LEED. The surface cleanliness was monitored by STM, AES, and valence band phoetoelectron spectroscopy (PES). MgO was deposited directly in situ from a W-crucible heated by electron bombardment. The base pressure in the vacuum chamber was 1×10^{-10} mbar and increased up to 1×10^{-9} mbar during the MgO deposition.

3 Results and discussion

Figure 1 shows LEED images of (a) a clean 50-Å-thick Fe(110) film as well as (b) a 30-Å-thick MgO(111) layer on top of the Fe(110) film. Very sharp (1×1) LEED patterns of bcc Fe(110) have been observed confirming the high surface quality of the epitaxial iron films (Fig. 1a). A well-ordered hexagonal (1×1) LEED pattern is clearly visible after the deposition of the nominal 30-Å-thick MgO layer. For intermediate thicknesses (5–30 Å) of MgO on top of the Fe(110) film the LEED images do not show any well-ordered structure, which means that a smooth transition from the bcc (1×1) structure to the fcc (1×1) structure takes place. The LEED spots during this structural transition are very weak or not visible, with a diffuse background (not shown here).

Figure 2a shows AES spectra for different coverages of MgO on top of the Fe(110) film. As the MgO layer thickness increases from 0 to 30 Å the intensity of the Fe $M_{2,3}$VV Auger peak decreases but its position does not change. At a MgO thickness of more than 50 Å the Fe Auger peak splits into two components. The AES spectra for 50 and 75 Å MgO on top of Fe(110) show peaks (see inset in Fig. 2a) which are characteristic of the presence of a significant amount of Fe in the oxidized state [24]. Generally, the detection of an iron oxide layer at the MgO/Fe interface is very difficult or not possible because the thickness of such a layer might be very small. Traditional spectroscopic techniques, such as XPS or AES, should in principle be able to identify a chemically shifted component related to the oxidized Fe surface atoms. However, the small shifted component must be resolved with respect to the large bulk metal contribution. The chemical shift for Fe interface atoms due to the interaction with the oxygen ions of the first MgO layer should be also taken into account. In presented experiments the Fe $M_{2,3}$VV AES peaks of iron oxide could only be observed after the deposition of more than 30 Å of MgO. In this case the iron oxide at the MgO/Fe interface is thick enough to give a significant contribution to the AES signal.

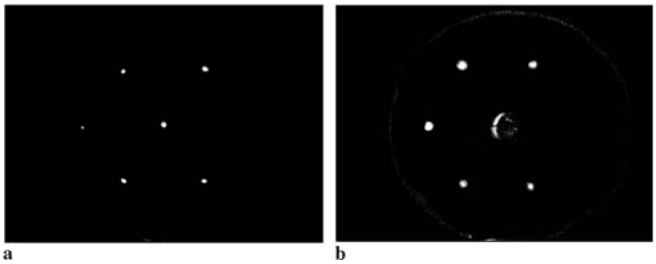

FIGURE 1 LEED images of (**a**) a 50-Å-thick Fe(110) film on a W(110) substrate and (**b**) a 30-Å-thick MgO(111) film on top of the Fe(110) film. The energy of the primary electron beam was 123 eV for (**a**) and 104 eV for (**b**) (the sixth spot in both pictures is not visible due to the sample holder)

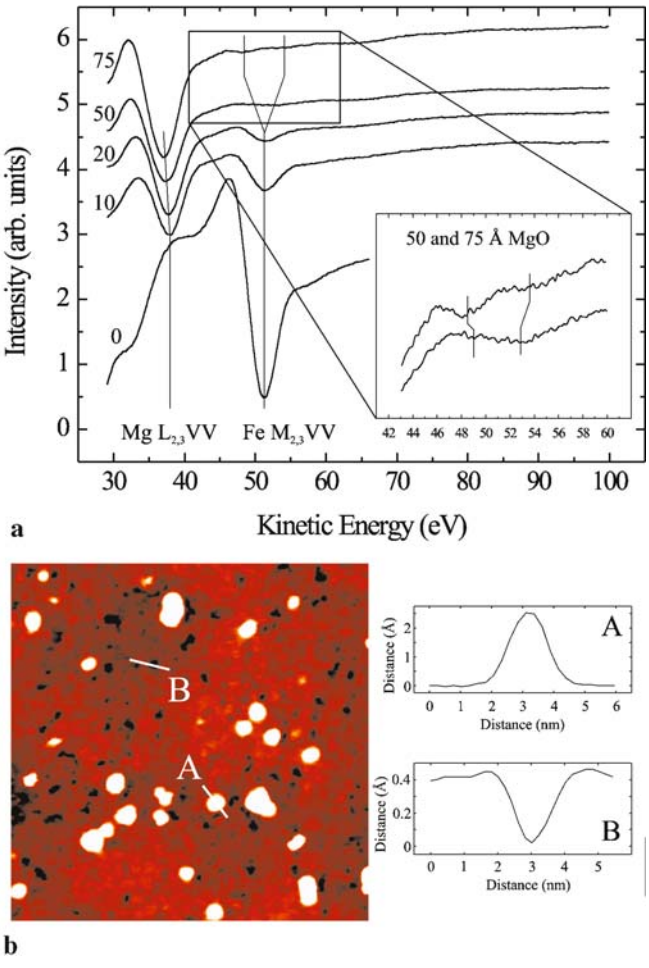

FIGURE 2 (**a**) AES spectra of the MgO/Fe(110) system as a function of MgO layer thickness. The MgO layer thickness in Å is marked on the *left-hand side* of each spectra. The *inset* shows zoomed spectra for 50 and 75-Å-thick MgO film on top of Fe(110). (**b**) A $50 \times 50\,\mathrm{nm}^2$ STM image of the Fe(110) surface after the deposition of nominal 0.3 Å of MgO. Tunneling parameters: 1.3 V, 1 nA. Profiles A and B correspond to STM height profiles along the *lines* shown in (**b**)

Figure 2b shows a $50 \times 50\,\mathrm{nm}^2$ STM image of the Fe(110) surface after the deposition of nominal 0.3 Å MgO. The MgO deposition on the Fe(110) surface leads to the formation of small MgO islands of undefined shape (white spots in Fig. 2b) which are uniformly distributed over the Fe(110) surface. The average height of the MgO islands was measured to be 2.1–2.5 Å (see height profile A in Fig. 2b). Along with the MgO islands small depressions are visible on the Fe(110) surface (dark spots in Fig. 2b). The depth of such depressions was measured to be 0.4–0.6 Å (height profile B in Fig. 2b). The observed depressions were found to be stable upon STM bias voltage variation in the range of 0.5–3.5 V. Such depressions were not observed on the pure Fe(110) surface before

MgO evaporation; therefore, they are unlikely to be a result of contamination. Thus, they may correspond to the partially oxidized Fe(110) surface. However it is difficult to estimate to what extent the Fe(110) surface is influenced by intermixing with MgO or by formation of a specific oxide layer at MgO/Fe(110) interface only on the basis of STM studies.

The modification of the electronic structure of the MgO/Fe(110) system as a function of the thickness of the deposited MgO layer was also investigated by means of photoelectron spectroscopy in normal emission. The PES spectra obtained in this experiment are shown in Fig. 3. They exhibit a pronounced structure corresponding to the emission from the Fe ($3d$) states in the range of binding energies near E_F as well as from the O ($2p$) states in the range of 4–10 eV. With an increasing amount of deposited MgO a gradual shift of the maxima of the O ($2p$) states and the valence band edge (VBE) towards larger binding energies can be clearly seen in Fig. 3. In the inset of Fig. 3 the change of the onset of the VBE position is shown with increasing MgO layer thickness. This shift is approximately 1 eV towards higher binding energy. As discussed by Kiguchi et al. [25] for the MgO/Ag(001) system this effect can be attributed to the increase of the binding energy of the Mg ($3s$) states above E_F and the increase of the binding energy of the O ($2p$) states, which results from the change in the Madelung potential for thin films.

The spin-resolved electronic structure of the MgO/Fe(110) system was investigated by SPARPES. The spin-resolved photoemission spectra together with the total emission intensity and the spin polarization as a function of the binding energy of Fe(110), 2 Å MgO/Fe(110) as well as 5 Å MgO/Fe(110) are presented in the left panel of Fig. 4 (from bottom to top) and in the right panel of Fig. 4, respectively. The spin-resolved spectra of the valence band of the Fe(110) film show the emission from the $\sum^1\downarrow\oplus\sum^3\downarrow$ states near 0.25 eV and from the $\sum^1\uparrow\oplus\sum^4\uparrow$ states near 0.7 eV. The value of the spin polarization of about $(-80\pm5\%)$ and the shape of the spectra are in agreement with previous measurements [23]. After the deposition of a 2-Å-thick MgO layer on the Fe(110) film surface the total intensity of the photoemission spectra measured near E_F decreases drastically. At the same time, the features of the valence band of Fe can still be observed. For this system the spin polarization near E_F is decreased to about $-(52\pm5)\%$ compared to $-(80\pm5)\%$ for the clean Fe(110) surface. Additional deposition of MgO on top of the Fe(110) film leads to a further decrease of the spin polarization at E_F (shown for the 5 Å MgO/Fe(110) system in Fig. 4 with $P(E_F)=-(21\pm5)\%$).

Figure 5 shows the experimentally determined changes of the normalized spin polarization at E_F of the MgO/Fe(110) system as function of the deposited MgO layer thickness. The spin polarization shows an unusual rapid decrease for MgO overlayer thickness up to 6 Å. The presented spin-resolved measurements (Fig. 4) reveal that the attenuation of the direct transition from the $\sum^1\downarrow\oplus\sum^3\downarrow$ bands near 0.25 eV is stronger than the one from the $\sum^1\uparrow\oplus\sum^4\uparrow$ states near 0.7 eV. This attenuation cannot be simply related to the difference in the spatial symmetry of the initial state photoelectron wave functions, but can rather be due to different group velocities of the electrons in the final $\sum^1$ state for $h\nu=21.2$ eV [26, 27]. Moreover, there are no MgO-related states overlapping with the initial Fe-related states, since bulk MgO is an insulator with a band gap of 7.8 eV. For ultra-

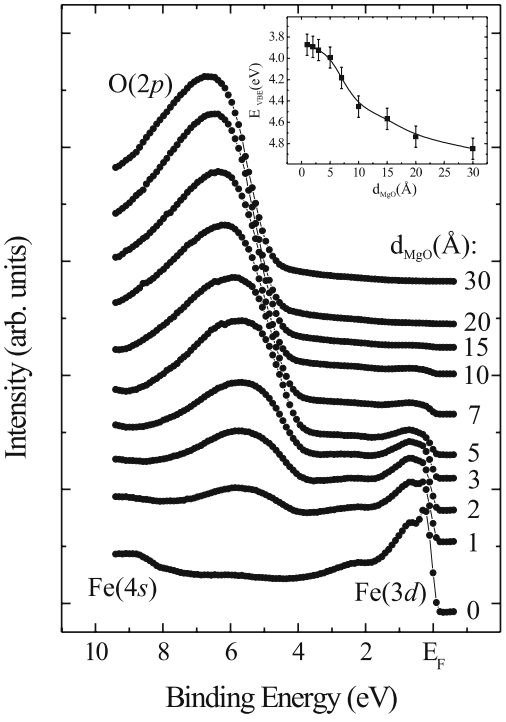

FIGURE 3 PES spectra ($h\nu=21.2$ eV) of the MgO/Fe(110) system as a function of MgO layer thickness. The *inset* shows the change of the valence band edge position of O ($2p$) states with increasing MgO thickness for the MgO/Fe(110) system

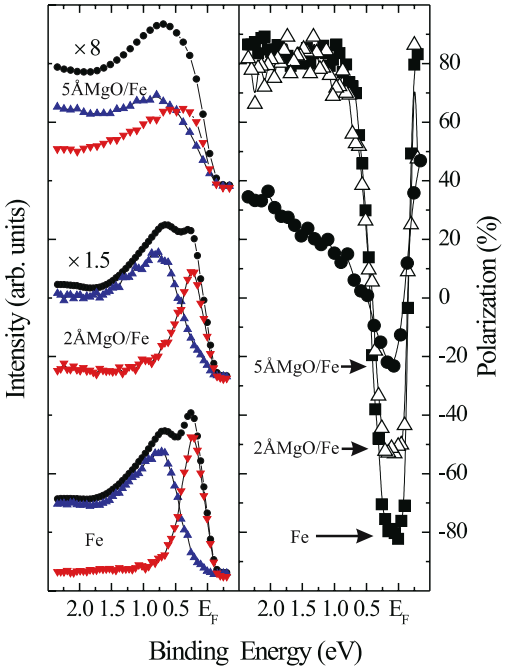

FIGURE 4 *Left panel*: The spin-resolved photoemission spectra (spin down: *triangle down*, spin up: *triangle up*) together with the total emission intensity (*solid circle*) of Fe(110), 2 Å MgO/Fe(110), and 5 Å MgO/Fe(110) (from bottom to top). *Right panel*: The spin polarization as function of binding energy of a 50-Å thick Fe(110) film (*solid square*), 2 Å MgO/Fe(110) (*open triangle up*), and 5 Å MgO/Fe(110) (*solid circle*)

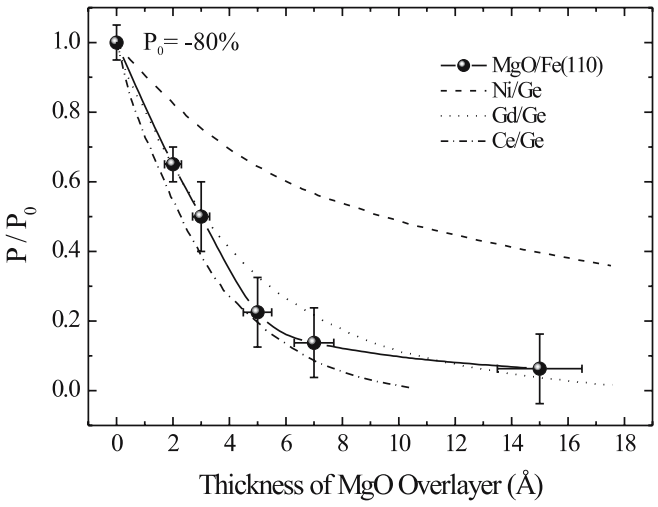

FIGURE 5 The change of the normalized spin polarization at E_F of the MgO/Fe(110) system with increasing MgO layer thickness. The spline fit to the experimental data is shown by a *solid line*. The reference curves for depolarization of polarized electrons ($P_0 = 23.5\%$) optically excited in germanium after traversing an evaporated overlayer of Ni (*dashed line*), Gd (*doted line*), and Ce (*dot-dashed line*) are taken from Ref. [29]

thin layers of MgO Klaua et al. [28] measured a tunneling barrier height with a minimum value of 2.6 eV for 2 ML of MgO. Assuming that the Fermi level is located approximately in the middle of the band gap, one can exclude any spectral weight from MgO in the region of 2 eV below E_F, implying no attenuation of the spin polarization as a function of MgO thickness.

Several different mechanisms may explain the observation of the rapid decrease of the spin polarization in the vicinity of the Fermi level. First, formation of interface states and the scattering of the excited photoelectrons at the interface and within the MgO layer may take place, which can be taken into account only by a proper one-step photoemission calculation.

The next, and more probable, mechanism relates to the formation of an ultrathin depolarizing interface layer of FeO at the MgO/Fe(110) interface. In this case, Zhang et al. [16] predicted a charge transfer and an induced magnetic moment of $0.19\,\mu_B$ at the oxygen atoms of the interfacial ultrathin FeO layer. Thus, one can assume that the spin-split density of states at the MgO/FeO/Fe(110) interface will be altered, giving rise to an additional spin-dependent scattering contribution. The latter could be due to scattering of spin-polarized electrons at hole states in the $3d$ shell of Fe^{2+} in the FeO interface layer[1]. The role of such a scattering process is illustrated by the reference curves in Fig. 5 taken from [29]. In Fig. 5 the exponential fits of the experimentally observed depolarization of polarized electrons ($P_0 = 23.5\%$) excited by circularly polarized light ($h\nu = 3.05$ eV) in germanium after traversing an evaporated overlayer of Ni (dashed line), Gd (dotted line), and Ce (dot-dashed line) are shown. All curves show an exponential dependence of the polarization on the thickness of the overlayer possessing d-electrons at E_F in the valence band. The mean free path for spin-flip scattering decreases as a function of the number of unoccupied d states in the valence band from Ni via Gd to Ce (Ni: two unoccupied d orbitals, $4s^2 3d^8$; Gd: nine unoccupied d orbitals, $6s^2 5d^1$; Ce: ten unoccupied d orbitals, $6s^2 5d^0$) [29]. The reference curves for the Gd/Ge and Ce/Ge systems are very close to the experimentally observed sharp decrease of spin polarization in the case of the presented MgO/Fe(110) system and can qualitatively be used as additional argument for the presence of a depolarizing FeO layer at the MgO/Fe(110) interface [spin-scattering into the four unoccupied d orbitals of Fe^{2+} ($3d^6$) in FeO]. The comparison is only qualitative with respect to the absolute number of hole states; there may be additional spin-scattering at the FeO/MgO interface. The presence of such a FeO interfacial layer and the increase of the FeO layer thickness at the MgO/Fe interface with increasing MgO layer thickness is supported by above presented AES and STM results.

[1] The formation of a spin-attenuating effect of a FeO(111) layer on top of Fe(110) has been observed previously, Y.S. Dedkov et al., Phys. Rev. B **65**, 064417 (2002).

4 Conclusion

In conclusion, the growth process of thin MgO films on epitaxial Fe(110) films and the electronic structure of the MgO/Fe(110) interface have been investigated. SPARPES experiments show that the spin polarization of a Fe(110) thin film drastically decreases with increasing MgO film thickness. The most probable mechanism to explain such behavior is spin scattering at $3d$-hole states of Fe^{2+} in connection with the formation of an ultrathin FeO layer at the MgO/Fe(110) interface. The presence of such a FeO interfacial layer and the increase of the FeO layer thickness at the MgO/Fe interface with increasing MgO layer thickness is supported by AES and STM results.

REFERENCES

1 J.S. Moodera, L.R. Kinder, T.M. Wong, R. Merservey, Phys. Rev. Lett. **74**, 3273 (1995)
2 T. Miyazaki, N. Tezuka, J. Magn. Magn. Mat. **139**, L231 (1995)
3 S. Yuasa, A. Fukushima, T. Nagahama, K. Ando, Y. Suzuki, Jap. J. Appl. Phys. **43**, L588 (2004)
4 S.S.P. Parkin, C. Kaiser, A. Panchula, P.M. Rice, B. Hughes, M. Samant, S.-H. Yang, Nature Materials **3**, 862 (2004)
5 S. Yuasa, T. Nagahama, A. Fukushima, Y. Suzuki, K. Ando, Nature Materials **3**, 868 (2004)
6 W.J. Gallagher, S.S.P. Parkin, Y. Lu, X.P. Bian, A. Marley, K.P. Roche, R.A. Altman, S.A. Rishton, C. Jahnes, T.M. Shaw, G. Xiao, J. Appl. Phys. **81**, 3741 (1997)
7 S.S.P. Parkin, K.P. Roche, M.G. Samant, P.M. Rice, R.B. Beyers, R.E. Scheuerlein, E.J. O'Sullivan, S.L. Brown, J. Bucchigano, D.W. Abraham, Y. Lu, M. Rooks, P.L. Trouilloud, R.A. Wanner, W.J. Gallagher, J. Appl. Phys. **85**, 5828 (1999)
8 H. Boeve, J. De Boeck, G. Borghs, J. Appl. Phys. **89**, 482 (2001)
9 M. Jullière, Phys. Lett. A **54**, 225 (1975)
10 J.M. MacLaren, X.G. Zhang, W.H. Butler, X. Wang, Phys. Rev. B **59**, 5470 (1999)
11 P. Mavropoulos, N. Papanikolaou, P.H. Dederichs, Phys. Rev. Lett. **85**, 1088 (2000)
12 I.I. Oleinik, E.Y. Tsymbal, D.G. Pettifor, Phys. Rev. B **62**, 3952 (2000)
13 W.H. Butler, X.G. Zhang, T.C. Schulthess, J.M. MacLaren, Phys. Rev. B **63**, 054416 (2001)
14 M. Bowen, V. Cros, F. Petroff, A. Fert, C. Martínez Boubeta, J.L. Costa-Krämer, J.V. Anguita, A. Cebollada, F. Briones, J.M. de Teresa, L. Morellón, M.R. Ibarra, F. Güell, F. Peiró, A. Cornet, Appl. Phys. Lett. **79**, 1655 (2001)
15 J. Faure-Vincent, C. Tiusan, E. Jouguelet, F. Canet, M. Sajieddine, C. Bellourad, E. Popova, M. Hehn, F. Montaigne, A. Schuhl, Appl. Phys. Lett. **83**, 4507 (2003)

16 X. Zhang, W.H. Butler, A. Bandyopadhyay, Phys. Rev. B **68**, 092 402 (2003)
17 H.L. Meyerheim, R. Popescu, J. Kirschner, N. Jedrecy, M. Sauvage-Simkin, R. Pinchaux, Phys. Rev. Lett. **87**, 076 102 (2001)
18 H.L. Meyerheim, R. Popescu, N. Jedrecy, M. Vedpathak, M. Sauvage-Simkin, R. Pinchaux, B. Heinrich, J. Kirschner, Phys. Rev. B **65**, 144 433 (2002)
19 H. Oh, S.B. Lee, J. Seo, H.G. Min, J.-S. Kim, Appl. Phys. Lett. **82**, 361 (2003)
20 S.K. Purnell, X. Xu, D.W. Goodman, B.C. Gates, J. Phys. Chem. **98**, 4076 (1994)
21 T.T. Magkoev, G.G. Vladimirov, D. Remar, A.M.C. Moutinho, Solid State Commun. **122**, 341 (2002)
22 R. Raue, H. Hopster, E. Kisker, Rev. Sci. Instrum. **55**, 383 (1984)
23 R. Kurzawa, K.-P. Kämper, W. Schmitt, G. Güntherodt, Solid State Commun. **60**, 777 (1986)
24 J.L. Vassent, M. Dynna, A. Marty, B. Gilles, G. Patrat, J. Appl. Phys. **80**, 5727 (1996)
25 M. Kiguchi, T. Goto, K. Saiki, T. Sasaki, Y. Iwasawa, A. Koma, Surf. Sci. **512**, 97 (2002)
26 K.B. Hathaway, H.J.F. Jansen, A.J. Freeman, Phys. Rev. B. **31**, 7603 (1985)
27 A. Rampe, G. Güntherodt, D. Hartmann, J. Henk, T. Scheunemann, R. Feder, Phys. Rev. B. **57**, 14 370 (1998)
28 M. Klaua, D. Ullmann, J. Barthel, W. Wulfhekel, J. Kirschner, R. Urban, T.L. Monchesky, A. Enders, J.F. Cochran, B. Heinrich, Phys. Rev. B. **64**, 134 411 (2001)
29 F. Meier, G.L. Bona, S. Hüfner, Phys. Rev. Lett. **52**, 1152 (1984)